

In the Quest of Low-Frequency Impedance Spectra of Efficient Perovskite Solar Cells

Daniel Prochowicz, Suverna Trivedi, Nishi Parikh, Michael Saliba, Abul Kalam, Mohammad Mahdi Tavakoli,* and Pankaj Yadav*

Measurement and understanding of electrochemical impedance spectroscopy of perovskite solar cells (PSCs) are nontrivial, as perovskite absorbers are a mixed conductor exhibiting both ionic and electronic motion. Moreover, the interpretation of the low-frequency spectra especially low-frequency resistance (R_{LF}) is ambiguous. Some reports suggest that R_{LF} is related to ionic transport resistance, whereas others attribute it with the recombination processes. Herein, more light is put on the quest of low-frequency impedance spectra of efficient PSCs. It is found that high- and low-frequency resistances (R_{HF} and R_{LF}) follow a similar dependence on the applied bias and illumination with a comparable slope. These resistances are associated with the recombination processes in PSCs. The relation between low-frequency spectra of PSCs and the physical parameters such as the role of the interface, grains' sizes, and perovskite composition is studied. It is found that the low-frequency spectra of PSCs mainly depend on the grains' sizes and shift toward the high frequency, i.e., toward faster time constants with increasing the grain size. It is observed that these devices exhibit the lower recombination and higher open-circuit voltage. A convenient way for the in-depth analysis of PSCs, which will be crucial for designing better-performing PSCs, is provided.

1. Introduction

The field of photovoltaics has witnessed a tremendous success of organic–inorganic halide perovskites (OIHPs) over the past 10 years.^[1,2] This wide ranging family of semiconductors has propelled the power conversion efficiencies (PCEs) for solar cells to the current record of 25.5%^[3] due to its high absorption coefficient, long carrier diffusion length, high charge carrier mobilities, and a suitable bandgap.^[4–7] However, there is still a room for perovskite solar cells (PSCs) to achieve PCEs over 30% by increasing the open-circuit voltage (V_{OC}).^[8] For that, many studies have been devoted for a deeper understanding of the prevailing nonradiative recombination mechanisms, which is a key factor responsible for the reduction of V_{OC} .^[9]

The source of nonradiative recombination losses in perovskite cells still remains a hot topic of debate. With the help of electroluminescence spectroscopy, Grätzel and coworkers attributed the decrease in

Dr. D. Prochowicz
Institute of Physical Chemistry
Polish Academy of Sciences
Kasprzaka 44/52, Warsaw 01-224, Poland

Dr. D. Prochowicz
Department of Solar Energy
School of Technology
Pandit Deendayal Energy University
Gandhinagar, Gujarat 382007, India

Dr. S. Trivedi
Department of Chemical Engineering
National Institute of Technology
769008 Rourkela, India

N. Parikh
Department of Science
School of Technology
Pandit Deendayal Energy University
Gandhinagar, Gujarat 382007, India

Dr. M. Saliba
Institute for Photovoltaics (IPV)
University of Stuttgart
70174 Stuttgart, Germany

Dr. M. Saliba
Helmholtz Young Investigator Group FRONTRUNNER
Forschungszentrum Jülich
52425 Jülich, Germany

Dr. A. Kalam
Department of Chemistry
Faculty of Science
King Khalid University
P.O. Box 9004 Abha 61413, Saudi Arabia

Dr. M. Mahdi Tavakoli, Dr. P. Yadav
Department of Electrical Engineering and Computer Science
Massachusetts Institute of Technology
Cambridge, MA 02139, USA
E-mail: mtavakol@mit.edu; Pankaj.yadav@sse.pdpu.ac.in

 The ORCID identification number(s) for the author(s) of this article can be found under <https://doi.org/10.1002/ente.202100229>.

DOI: 10.1002/ente.202100229

V_{OC} to the nonradiative surface recombination because of nonselective contacts.^[10] The investigations by other measuring techniques such as time-resolved photoluminescence (TRPL) and transient absorption (TA) spectroscopy revealed that radiative recombination of free electrons and holes is a dominant for PL processes.^[11] A model involving surface photogenerated carriers for the recombination kinetics in PSCs was proposed by Zarazua et al.^[12] The authors concluded that surface recombination is the dominant process, which governs the reduction of both short-circuit current and V_{OC} , and the nonradiative recombination occurs mainly at the vicinity of the contacts. Contrary to this, in another report, the nature of recombination was studied using a combination of impedance spectroscopy experiments and voltage-illumination measurements under different conditions of temperature, excitation wavelength, and illumination directions.^[13] This study shows that the prevailing recombination mechanism arises from the bulk of the perovskite. Afterward, Tress et al. measured the temperature-dependent ideality factor and activation energy to better understand the mechanism, sources, and location of recombination.^[14] The detailed investigations carried out on devices with different architectures using light-intensity-dependent V_{OC} measurement revealed that 1) recombination is not much affected by the n-type contact in both planar and mesoporous architectures; 2) surface recombination is mainly dominated in devices without hole transport layer; and 3) bulk of the perovskite is generally responsible for recombination in case of the optimized device. Thus, the origin and mechanism of the recombination processes in PSCs requires further deeper understanding to ensure future advances.

Electrochemical impedance spectroscopy (EIS) has been proven to be a powerful tool to understand the kinetic processes occurring within an electrochemical system.^[15] However, the interpretation of EIS spectra is a complex process, as the perovskite material is a mixed conductor exhibiting both ionic and electronic transports. In general, the EIS of the PSCs features two arcs associated with the low and high frequencies. It was demonstrated that the ideality factor (recombination resistance) and the other electrical properties can be solely calculated from the high-frequency response.^[16–18] In contrast, the low-frequency components, resistance (R_{LF}) and capacitance (C_{LF}), arise from the charging and discharging of the Debye layers because of the ion vacancy motion.^[19] Thus, the C_{LF} is mainly interpreted as the accumulation or apparent capacitance.^[14,20] However, the interpretation of R_{LF} is ambiguous. Some reports suggest that R_{LF} is related to ionic transport resistance,^[21] whereas in another report, R_{LF} was associated with recombination process as the behavior is the same as for the high-frequency resistance (R_{HF}).^[19] Hence, because of this ambiguity, the question arises whether the R_{LF} is associated with the recombination process and/or ionic transport.

Here, we experimentally shed more light on the quest of low-frequency impedance spectra in efficient PSCs. We confirm that high- and low-frequency resistances (R_{HF} and R_{LF}) follow a similar dependence on the applied bias and illumination with a comparable slope. We correlate both the resistances to be associated with the recombination process in PSCs. Moreover, we also confirm that the low-frequency capacitance (C_{LF}) and R_{LF} exhibit the similar slope but with the opposite dependence on the applied bias and illumination in line with the previous study by

Zarazua et al.,^[20] which signifies the electrical components are related to each other. These observations establish the fact that recombination in PSCs is mainly defined by the resistive elements, R_{HF} and R_{LF} , obtained from EIS spectra. In the next step, we rigorously analyze the EIS spectra to establish the dependence of low-frequency spectra of PSCs on the physical parameters such as the role of interface, grains' sizes, and perovskite compositions. To the best of our knowledge, the dependence of low-frequency impedance on these parameters is rarely discussed in the literature.^[22,23] We find that the low-frequency spectra of PSCs mainly depend on the grain size and devices with larger grain size exhibit lower recombination and higher open-circuit voltage. We found that an increase in grains' sizes shifts the low-frequency peak toward the higher frequency, i.e., toward faster time constant. This study provides a convenient way for in-depth analysis of PSCs, which will be crucial for designing better-performing PSCs.

2. Results and Discussion

2.1. Origin of the Low-Frequency Arc of EIS in PSC

In this section, a device with a planar configuration of fluorine-doped tin oxide (FTO)/TiO₂/perovskite/spiro-OMeTAD/Au was fabricated and investigated. The perovskite layer has a composition of Cs₅(MA_{0.17}FA_{0.83})₉₅Pb(I_{0.83}Br_{0.17})₃ and was deposited by one-step solution processing as recently reported.^[24] (For detailed experimental procedure refer the study by Yadav et al.^[24]) **Figure 1a** shows the current–voltage characteristic (J – V) of the champion device measured under AM 1.5 illumination. The measured device yields an open-circuit voltage (V_{OC}) of 1.16 V, short-circuit current (J_{sc}) of 23.2 mA cm^{−2}, fill factor (FF) of 71% and PCE of 19.1% which is close to the highest-performing PSCs.^[25,26] **Figure 1b** shows the EIS of the device measured as a function of illumination intensity, which are similar with the recent studies.^[16–18] The key EIS features that are commonly observed in PSCs are as follows: 1) under illumination two distinct semicircle arcs in the frequency range of 0.1–10 Hz (low-frequency spectra) and 10⁵–10⁶ Hz (high-frequency spectra) are observed; 2) the time response of low-frequency spectrum is found to be illumination independent and bias dependent; 3) the rate of change in the resistive part of low- and high-frequency spectra is almost same under illumination. **Figure 1c** shows the electrical equivalent circuit used to fit the obtained EIS spectra. **Figure S1**, Supporting Information, shows the fitting of the obtained EIS spectra using an electrical equivalent circuit. The electrical equivalent circuit consists of R_s , which accounts the series resistance of connecting wire and ohmic resistance of PSCs. Apart from the R_s , this circuit also contains the resistance from the low- (R_{LF}) and high- (R_{HF}) frequency spectra. In the literature, it is frequently reported that R_{HF} is physically related to the recombination processes in PSCs.^[27,28] The value of ideality factor (which defines the recombination) of PSCs can be obtained by plotting the value of R_{HF} as a function of applied bias or illumination.^[29] At the same time, the detailed physical interpretation of R_{LF} is still a topic of debate in literature. It was claimed that R_{LF} is due to the ionic transport resistance as its value changes according

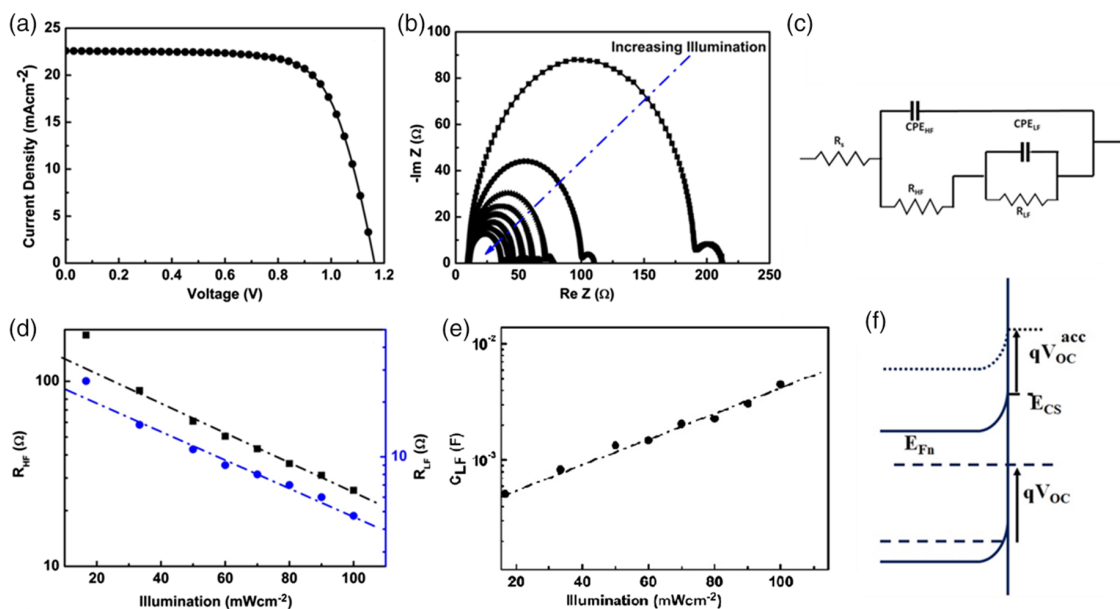


Figure 1. a) J - V characteristic of the best-performing device measured with a scan rate of 150 mV s^{-1} (reverse scan); b) EIS of device as a function of illumination; c) electrical equivalent circuit; d) resistance plot of low (blue) and high frequency (black) as a function of illumination at V_{OC} ; e) capacitance plot extracted from the low-frequency spectra as a function of illumination at V_{OC} ; and f) band bending in PSCs at open circuit.

to the diffusion and concentration of mobile ions. Moreover, R_{LF} can be also ascribed to the recombination process in PSCs, as it behaves the same as R_{HF} under bias and illumination.^[23] In other works, R_{LF} was attributed to ionically modulated recombination, where recombination is induced and lead by ions motion and position.^[30,31] The shown capacitance in the electrical equivalent circuit has been interpreted as follows: the high-frequency capacitance C_{HF} (in the frequency range of $>10^3 \text{ Hz}$) is defined as a geometrical capacitance, the dielectric of perovskite absorber layer defines this capacitance as $C_{HF} = \epsilon_0 \epsilon / d$, where ϵ_0 is the permittivity of free space, ϵ and d is dielectric and thickness of perovskite absorber layer, respectively. The capacitance C_{LF} associated with the low frequency ($\approx 10^{-1} \text{ Hz}$) is associated with the ionic phenomena. C_{LF} is also known as interface accumulation capacitance, which is found to be ionic under dark condition and electronic under illumination.^[12] To study the relation between the electrical equivalent circuit components, EIS spectra as a function of illumination are fitted with the electrical equivalent circuit shown in Figure 1c. Figure 1d shows the variation of R_{HF} and R_{LF} as a function of illumination, which shows similar dependence on illumination with an almost similar slope. This suggests that both the resistances are from the same physical phenomena, as already proposed in previous studies.^[16–18] The significant reduction in value is observed for R_{HF} , as it reduces from 180Ω at low illumination to 30Ω at 1 sun illumination, whereas R_{LF} decreases from 100 to 10Ω .

Recent studies have shown that both the resistances (low and high frequencies) describe the process related to electron and hole recombinations.^[27] It was also found that these resistances have a strong voltage and illumination dependence, as charge carrier density changes linearly with the change in illumination. A similar observation is also illustrated by work of Zarazua

et al., in which two resistances (low and high frequencies) exhibit extremely similar behavior (decreasing) as a function of light intensity and photovoltage, suggesting a common origin for both the resistances.^[12] However, Riquelme et al. have shown that the R_{HF} (not R_{LF}) can be considered as a true recombination resistance as both the resistances have different biases and illumination dependences.^[19] Moreover, a similar slope, but with the opposite trend, is observed between R_{LF} and C_{LF} here, which indicates the same physical origin among them, but not with R_{HF} . Based on our results and studies from the other authors following points are drawn: 1) R_{HF} and R_{LF} follow a similar dependence on the applied bias and illumination with a comparable slope. This signifies that both the resistances stem from the same physical origin, which is associated with the recombination in PSCs; 2) C_{LF} and R_{LF} exhibit a similar slope but with the opposite dependence on the applied bias and illumination, which signifies the same physical process. The low-frequency capacitance is associated with accumulation of electronic charge carriers (see the next section for a more detailed discussion) and therefore one can relate the R_{LF} to the recombination of accumulated electronic charges; 3) The recombination in PSCs is mainly defined by the resistive elements R_{HF} and R_{LF} , which are found to be connected with the C_{LF} .

An illumination-independent behavior of C_{HF} with an approximate value of $5\text{--}10 \mu\text{F}$ is shown in Figure S2, Supporting Information. In contrast, the value of C_{LF} increases with increasing the illumination, as shown in Figure 1e. Recently, C_{LF} was interpreted as a purely ionic in nature, which forms an ionic Debye length in perovskite absorber layer as $L_D = \sqrt{\frac{\epsilon_p V_T}{N_0 q}}$, where ϵ_p is the permittivity of the perovskite absorber layer, N_0 is the density of ion vacancies, V_T is the thermal voltage, and q is the

electronic charge.^[32,33] Considering only the ionic charge stored in the Debye layer, the resultant capacitance is limited by the Helmholtz capacitance, which in practice cannot be considerably higher than $\mu\text{F cm}^{-2}$. In such a case, under illumination, the obtained value of C_{LF} is not only lead by the ionic accumulation but also involves the electronic charge accumulation.^[20] In this situation, the expression for Debye length is modified as $L_D = \sqrt{\frac{\epsilon_p V_T}{p_o q}}$, where p_o majority hole concentration. The bias dependence of accumulated majority charge carriers and corresponding capacitance is given as $p_{\text{acc}} = p_o L_D \sqrt{2} e^{qV/2k_B T}$ and $C_{\text{acc}} = \frac{\epsilon \epsilon_o}{\sqrt{2} L_D} \exp\left(\frac{qV}{2k_B T}\right)$. From this expression, an exponential dependence of capacitance on the applied potential or illumination with a slope of $\frac{1}{2k_B T}$ is expected. Using the expression of capacitance and obtained plot of C_{LF} with change in illumination level, a positive slope is obtained. Importantly, it should be noted here that the extent of accumulation of charge carriers under illumination is kinetically control by the ion distribution inside the perovskite layer. Figure 1f shows the band bending of PSCs at 1 sun illumination in V_{OC} condition; the figure is drawn based on the various simulation studies by other authors.^[12,20] The total potential drop across the perovskite absorber layer is simply defined as the total potential drop across device minus drop across the Debye layers. This is represented as $E_{\text{Bulk}} = \frac{(V_{\text{bi}} - V_{\text{app}}) - v_+ - v_-}{t}$, where V_{bi} is built in potential, V_{app} applied potential across the device, v_+ potential drop across hole transporting layer (HTL)/perovskite interface, v_- potential drop across electron transporting layer (ETL)/perovskite interface, and t thickness of perovskite absorber layer. Considering the operation of PSC above the flat band condition, i.e., beyond V_{bi} in this situation, the net electric field across the perovskite absorber layer

is negative and causes the positive and negative ions move toward the ETL/perovskite and HTL/perovskite interfaces.^[12] In this scenario, the formation of C_{LF} (if only ions are considered) is limited by the Helmholtz with a maximum limits in $\mu\text{F cm}^{-2}$. The obtained experimental C_{LF} (Figure 1e) value in the order of mF cm^{-2} is supported by the accumulation of electronic charge carrier. The electronic accumulation is mainly associated with holes, which cause a upward band bending at ETL/perovskite interface (Figure 1f). The physical phenomena of the increase in the accumulation of electronic charges at interface, i.e., C_{LF} is related to the recombination at interface, as R_{HF} and R_{LF} are linked inversely with the C_{LF} . Thus, EIS of PSC mainly depicts the information of recombination and charge accumulation via R_{HF} , R_{LF} , and C_{LF} , respectively. In the further sections, the dependence of low-frequency spectra of PSCs on the physical parameters such as role of interface, grain boundaries, and perovskite composition will be discussed.

2.2. Effect of ETL/Perovskite Interface Engineering on the Low-Frequency Arc in EIS of PSC

In general, the ETL/perovskite interface mainly dominates the charge accumulation and capacitance, as HTL/perovskite interface is ohmic in nature.^[20] To study the role of the interface on the low-frequency parameters (R_{LF} , C_{LF}) and associated time constants, we modified the ETL/perovskite interface by depositing a thin layer of ZnO and SnO_2 over TiO_2 ETL. (For detailed experimental procedure, refer the studies by Yadav and coworkers.^[34,35] The results of the devices studied here are from the same batch as in the studies by Yadav and coworkers.^[34,35] The modification of ETL led to an increase in V_{OC} and FF of the devices, as reported in our previous studies.^[34,35] The EIS of the devices were measured at bias above the V_{bi} of PSCs, as in this region, the net response of

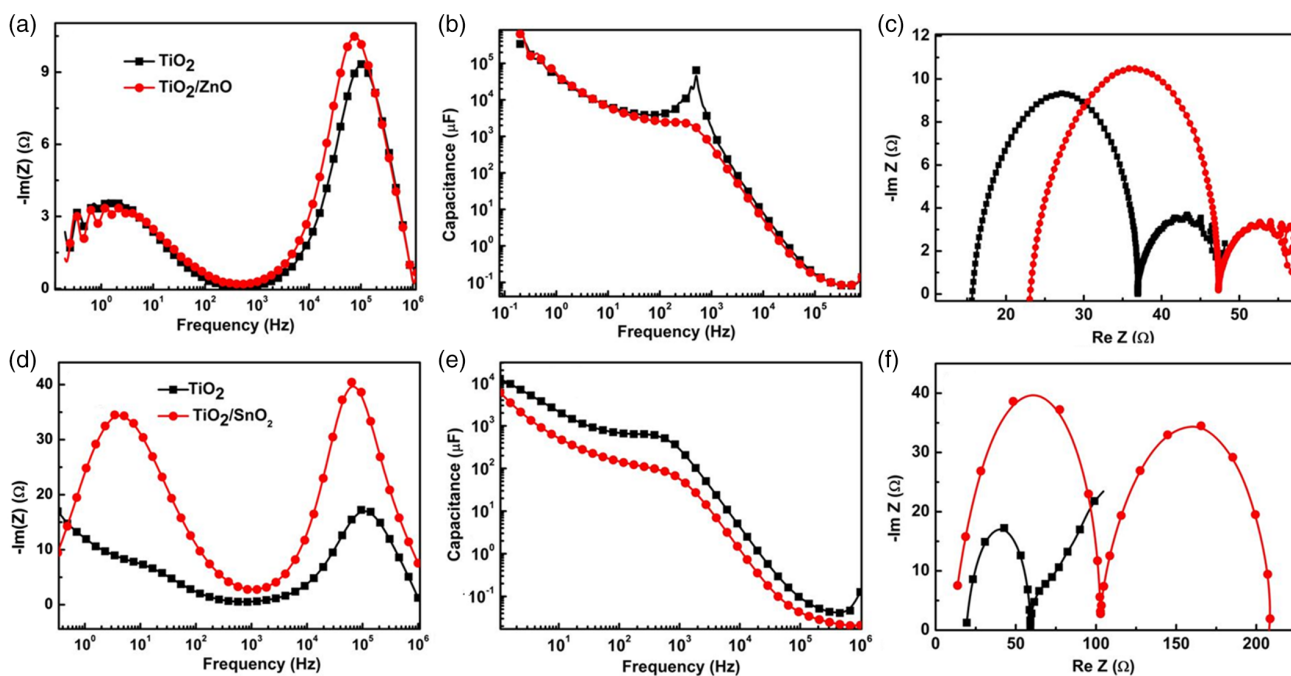


Figure 2. a) $-\text{Im}(Z)$ versus frequency plot, b) capacitance versus frequency plot, c) Nyquist plot for TiO_2 and TiO_2/ZnO PSCs. d) $-\text{Im}(Z)$ versus frequency plot, e) capacitance versus frequency plot, and f) Nyquist plot for TiO_2 and $\text{TiO}_2/\text{SnO}_2$ PSCs.

the device is mainly because of recombination rather than charge injection. Figure 2a–c shows the $\text{Im}(Z)$ versus frequency, capacitance versus frequency, and EIS response of pristine TiO_2 and TiO_2/ZnO ETL-based PSCs, respectively. In Figure 2a, both the devices show the low- and high-frequency peaks with a similar frequency range. The low-frequency peak in the frequency range of $\approx 1\text{--}10$ Hz is observed in both the devices. The time response associated with the low-frequency peak is calculated as $\tau_{\text{LF}} = R_{\text{LF}}C_{\text{LF}}$, or by taking the inverse of frequency peaks in $\text{Im}|Z|$ versus frequency plots, which is found to be close to 1 s in both the devices. The capacitance response of both the devices also illustrates the similar response to frequency, which signifies that the accumulations of charges are almost similar in both the devices, or similar amount of charges are available at the interface for recombination (Figure 2b). However, looking at the net resistance of PSCs in Figure 2c (without series resistance), a higher value of R_{HF} and R_{LF} is obtained for TiO_2/ZnO ETL-based device, suggesting lower recombination. The observed lower recombination in TiO_2 surface-treated devices leads to a higher value of photovoltage.

To further confirm these results, TiO_2 ETL was modified with a thin layer of SnO_2 . In Figure 2d, both devices show a similar dependence on the change in frequency, but with a difference in magnitude. From Figure 2a,d, it is concluded that the treatment of the ETL layer has the least impact on the position of the low- and high-frequency peaks in $-\text{Im}(Z)$ versus frequency plots. Interestingly, the treatment of TiO_2 ETL with SnO_2 layer leads to a decrease in the value of capacitance (Figure 2e). The reduction in the capacitance values was previously observed after Li^+ treatment of the TiO_2 layer.^[36] The authors found that the presence of Li^+ at ETL/perovskite interface could reduce the accumulation of the intrinsic ions, and especially avoid the interactions at ETL surface by reducing the density of holes.^[36]

In line with the results shown in Figure 2d, a higher value of R_{HF} and R_{LF} in $\text{TiO}_2/\text{SnO}_2$ PSC is obtained as compared with that of the reference device, which suggests lower recombination and higher value of V_{OC} (Figure 2f). In the case of $\text{TiO}_2/\text{SnO}_2$ PSC, lower recombination is expected as charge accumulation at interface, i.e., C_{LF} is lower than that found in TiO_2 PSC (Figure 2e). From the aforementioned analysis, it is clear that interpreting capacitance or resistance alone will not provide the exact information on the device physics. We note that obtained EIS spectra of TiO_2 PSCs in Figure 2c,f are different from each other. The plausible reasons for this are 1) the PCEs for both the cells are different; 2) as mentioned previously, the spectra are taken at knee voltage, the value of which is different in both the samples of TiO_2 PSCs. Hence, a difference in the EIS responses can be expected. However, more importantly, the interpretations of time constants from both the high- and low-frequency spectra are same. The reproducibility of photovoltaic parameters in their respective batches can be found in our previous work.^[34,35] Looking at the values of R_{HF} and R_{LF} of $\text{TiO}_2/\text{SnO}_2$ and TiO_2/ZnO PSCs, lower recombination and higher V_{OC} are expected for $\text{TiO}_2/\text{SnO}_2$ PSCs. Although the ZnO ETL has higher electron mobility, the remaining hydroxide (OH^-) surface ions on ZnO ETL can induce the degradation of perovskite absorber layer.^[37,38] In contrast, SnO_2 improves the band energy and band alignment because of the deep conduction band at the ETL/perovskite interface as reported in previous studies.^[39,40]

2.3. Effect of Grain Size and Boundaries in Perovskite Layer on the Low-Frequency Arc in EIS of PSC

Next, we have investigated the role of grain size and boundaries on the R_{LF} , C_{LF} , and associated time constants. To modify the grain size of the perovskite absorber layer, we have applied two different protocols. The first method involves the use of different antisolvents, isopropanol (IPA) and chlorobenzene (CB), to change the crystallization kinetics, which leads to distinct difference in the morphology. In another approach, we added CsCl to the perovskite precursors solution, as the beneficial role of chlorine on the morphology of perovskite is well reported.^[41,42] A detail of both the approaches and their effect on the photovoltaic parameters of PSCs are discussed in our previous works.^[41,42] Specifically, we demonstrated that the IPA-treated perovskite films have a more uniform, pin-hole-free surface morphology, and exhibits a larger grain size as compared with CB-treated thin films.^[41] Moreover, from atomic force microscopy (AFM) images, we found that root-mean-square (RMS) surface roughness of CB- and IPA-treated films are 33 and 18 nm, respectively.^[41] Figure 3a shows the plot of $-\text{Im}(Z)$ versus frequency plot of IPA- and CB-PSCs. Both the PSCs illustrate the similar trends in the low- and high-frequency regions. However, a difference in magnitude of $-\text{Im}(Z)$ is observed, which mainly originates from the difference in the magnitude of capacitance. A slight shift of the low-frequency peak toward higher values of frequency is observed in IPA- compared with CB-treated PSCs. Recent studies by Alvarez et al., have shown that the faster time response or kinetics lead to a behavior dominated by ionic diffusion.^[36] In the present case, faster ionic diffusion is expected in IPA-PSCs because of larger grains' sizes. This result signifies that the sizes of the grains affect the impedance response of PSCs. The capacitance spectra shown in Figure 3b exhibit an almost comparable value of capacitance in the high-frequency range for both the devices. Focusing on the low-frequency spectra (<10 Hz), a higher value of C_{LF} is obtained for the IPA-treated PSC (Figure 3b). In our previous work, we have shown that a significant difference in the value of C_{LF} is obtained with increasing the bias toward the V_{OC} of PSCs, which signifies the difference in the charge accumulation.^[41] While looking at the Nyquist spectra of both the devices, a mix response is obtained as IPA-treated PSC exhibits a higher value of R_{HF} and lower value of R_{LF} as compared with CB-treated PSCs (Figure 3c). As we observed in the previous section, both the resistances are associated with the same physical phenomena, i.e., recombination and both the resistances are connected in series with each other. It is more reasonable in practice to consider the recombination resistance of PSCs as $R_{\text{rec}} = R_{\text{HF}} + R_{\text{LF}}$.^[20] Moreover, with the increase in the bias toward V_{OC} of PSCs, the R_{LF} of CB-treated device decreases at a higher rate and shows a comparable value as compared with IPA-treated PSC. Full detail description of the EIS spectra is discussed in our previous report.^[41] We note that lower recombination in devices exhibiting higher grain size of perovskite absorber layer perovskite is already well established in the literature.^[43,44]

To further confirm the role of grain size on the low-frequency spectra of EIS, PSCs based on the $\text{Cs}_{0.20}\text{FA}_{0.80}\text{PbI}_3$ perovskite composition using CsI and CsCl are studied.^[37] We found that perovskite film of $(\text{Cs})_{0.20}(\text{FA})_{0.80}\text{PbI}_3\text{-(Cl)}$ using CsCl as a source

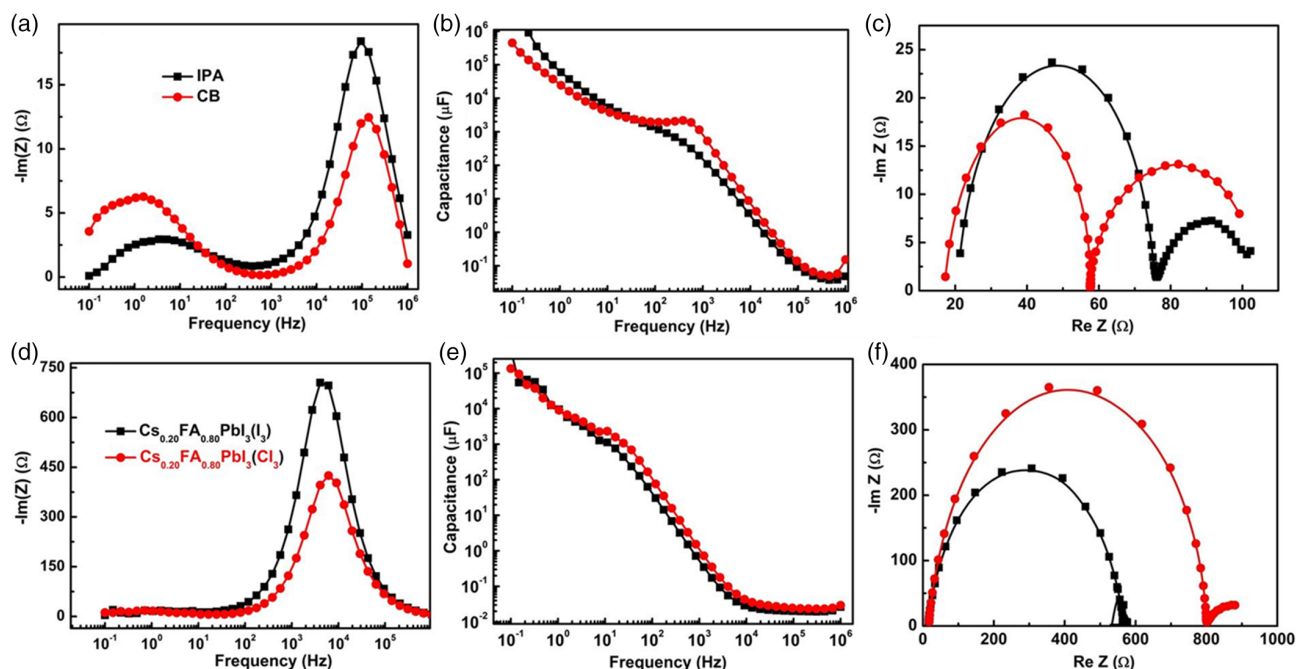


Figure 3. a) $-\text{Im}(Z)$ versus frequency plot; b) capacitance versus frequency plot; c) Nyquist plot for PSCs fabricated using IPA and CB; d) $-\text{Im}(Z)$ versus frequency plot; e) capacitance versus frequency plot; f) Nyquist plots for $(\text{Cs})_{0.20}(\text{FA})_{0.80}\text{PbI}_3\text{-(I)}$ and $(\text{Cs})_{0.20}(\text{FA})_{0.80}\text{PbI}_3\text{-(Cl)}$ PSCs.

of cesium cation exhibits much larger grain size (up to $\approx 1 \mu\text{m}$) as compared with the perovskite film $(\text{Cs})_{0.20}(\text{FA})_{0.80}\text{PbI}_3\text{-(I)}$ fabricated from a spin coating of a solution containing FAI, PbI_2 , and CsI in a certain stoichiometry.^[42] Figure 3d shows an almost similar trend of $-\text{Im}(Z)$ versus frequency plot for both the devices. We note that a small peak is obtained for $(\text{Cs})_{0.20}(\text{FA})_{0.80}\text{PbI}_3\text{-(Cl)}$ PSC at low-frequency area ($< 10 \text{ Hz}$) (Figure S3, Supporting Information), whereas no detectable peak is observed for $(\text{Cs})_{0.20}(\text{FA})_{0.80}\text{PbI}_3\text{-(I)}$ PSC. This result is consistent with the findings of IPA- and CB-PSCs, where faster time response or kinetics is obtained for absorber layer with larger grain size. Figure 3e shows that the value of C_{LF} is similar for both the devices.^[42] However, the decrease in recombination is clearly visible in the EIS spectra shown in Figure 3f, where significantly higher-resistive values is obtained for the $(\text{Cs})_{0.20}(\text{FA})_{0.80}\text{PbI}_3\text{-(Cl)}$ PSCs. The $(\text{Cs})_{0.20}(\text{FA})_{0.80}\text{PbI}_3\text{-(Cl)}$ device exhibits low-frequency EIS arc, which is masked by the high-frequency arc in the case of $(\text{Cs})_{0.20}(\text{FA})_{0.80}\text{PbI}_3\text{-(I)}$ PSCs.

Riquelme et al. have simulated the low-frequency spectra peak in $\text{Im}|Z|$ versus frequency plots, and showed that this peak shifts toward the high frequency as it is related to the high diffusion coefficient of ions.^[19] The authors also stated that the associated low-frequency resistance, i.e., R_{LF} should be the function of ions diffusion. Comparing the plots shown in Figure 2 and 3, it is established that shift in low-frequency peak in $\text{Im}|Z|$ versus frequency plots and value of R_{LF} and C_{LF} has a no direct relation. It is possible that the ion accumulation at interface under illumination increases recombination. At low frequency, ions at Debye layer have sufficient time to adjust with the applied perturbation and potential. Recognize that measured EIS spectra is obtained at the photovoltage, i.e., close to $V_{\text{OC}} > V_{\text{bi}}$ of PSC, this causes the

motion of holes and positive ions at ETL/perovskite interface and causes the energy levels uplift by creating the accumulated zone (ETL/perovskite interface) (Figure 1f). The accumulated ions further increase the potential of the Debye layer that causes the development of electrostatic potential.^[12] In this situation, the exact motion and accumulation of ions and charges and their dependence on grain size or chemical composition of the perovskite absorber layer and the resulting effect on low-frequency R_{LF} and C_{LF} are not yet clear. Various other measurements have also demonstrated that the slow response in PSCs is due to the ions but the kinetics of slow response on the charge accumulation and recombination is not fully established yet. Further experiments that will focus on understanding the slow response of ions along with charge carrier phenomena is urgently needed.

2.4. Effect of Perovskite Composition on the Low-Frequency Arc in EIS of PSC

In the next step, we discuss the role of A- and B-site cations in the ABX_3 perovskite structure on the low-frequency arc of EIS in PSCs. To study the role of A-site cation, we fabricated and studied the devices based on mixed-cation formulation of $\text{GUA}_x\text{MA}_{1-x}\text{PbI}_3$ ($\text{GUA} = \text{guanidinium}$).^[45] (For detailed experimental procedure, refer the study by Kubicki et al.^[45]) Figure 4a and Figure S4, Supporting Information, shows $\text{Im}|Z|$ versus frequency plots of MAPbI_3 and $\text{GUA}_{0.10}\text{MA}_{0.90}\text{PbI}_3$ (MAGUA) devices, respectively. We found that EIS spectra of both the devices exhibit a low-frequency peak at 10 Hz. In a closer look, it was observed that incorporation of GUA shifts the low-frequency peak toward the higher frequency. Recent studies have reported that GUA cation can form strong hydrogen bonds with the

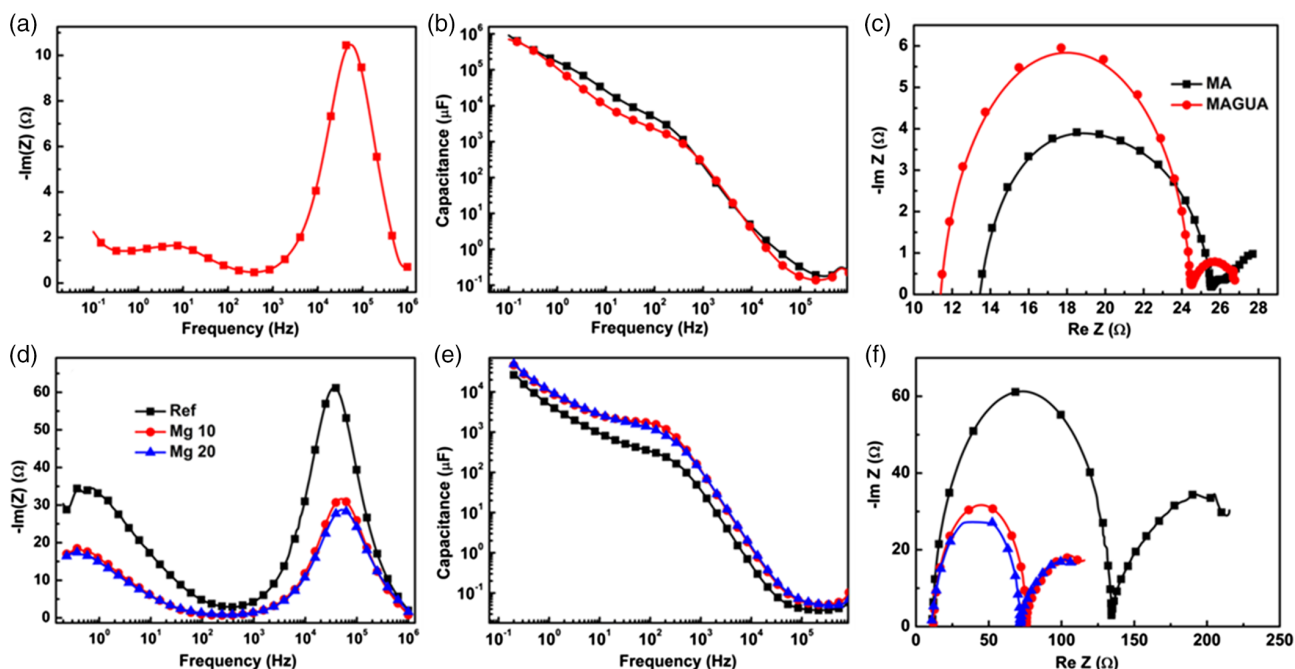


Figure 4. a) $-\text{Im}(Z)$ versus frequency plot of MAGUA PSC; b) capacitance versus frequency plot for MAPbI₃ and MAGUA PSCs; c) Nyquist plot for MAPbI₃ and MAGUA PSCs. d) $-\text{Im}(Z)$ versus frequency plot; e) capacitance versus frequency plot; and f) Nyquist plot for the CsMAFA and Mg-containing PSCs.

halides that may passivate the defects and improve the device performance.^[46,47] The capacitance response of MAPbI₃ and MAGUA devices depicts the similar frequency response in the low- and high-frequency regions, but C_{LF} increases significantly as bias approaches to V_{OC} for MAGUA PSC (see for more detail in the study by Kubicki et al.^[45]). In line with the results on IPA-treated PSCs, we also found that a higher value of C_{LF} not necessary leads to higher recombination. Exact information of recombination can be deduced from the resistive values. A higher value of R_{HF} and R_{LF} is obtained for MAGUA PSC as compared with MAPbI₃ PSC signifying its lower recombination (Figure 4c). The incorporation of GUA in MAPbI₃ not only increases the recombination resistance but also reduces the series resistances. It will be interesting for future studies to test the role of other large cations on the low-frequency spectra of EIS.

Moreover, we have also studied the role of B-site cation on the low-frequency spectra of EIS. Here as a reference, we have used triple A-site cation composition of Cs₅(MA_{0.17}FA_{0.83})₉₅Pb(I_{0.83}Br_{0.17})₃ (CsMAFA) as a perovskite absorber layer^[25] and replaced Pb²⁺ with 10% and 20% by weight of Mg²⁺. Figure 4d shows $-\text{Im}|Z|$ versus frequency plots of CsMAFA, Mg₁₀, and Mg₂₀ PSCs. The obtained plot of $-\text{Im}|Z|$ versus frequency for PSCs shows a similar trend with the same peak position in the low- and high-frequency regions. Focusing on the peak at the low frequency, it is stated that B-site cation plays an insignificant role on the peak position of the low-frequency spectra. Moreover, the incorporation of Mg²⁺ leads to an increase in C_{LF} (Figure 4e) and decrease in R_{LF} (Figure 4f). This could be attributed to the fact that Mg²⁺ can act as a defect site leading to higher charge accumulation and recombination simultaneously.

3. Conclusions

In summary, we have systematically probed the EIS of efficient PSCs to address the ambiguous and most debateable nature of low-frequency spectra of EIS. The presented results confirm the claims in literature reported that low R_{LF} is related to recombination process and not with the ionic transport resistance. We further confirm that high- and low-frequency resistances (R_{HF} and R_{LF}) follow a similar dependence on the applied bias and illumination with a comparable slope. We associate both resistances with the recombination process in PSCs. Moreover, this study also establishes the relation between low-frequency EIS of PSCs on the physical parameters such as the role of the interface, grains' sizes, and perovskite composition. We establish that the low-frequency spectra of PSCs mainly depend on the grains' sizes. The increase in grains' size shifts the low-frequency peak toward the high frequency, i.e., toward faster time constants. It was observed that these devices exhibit the lower recombination and higher open-circuit voltage.

Supporting Information

Supporting Information is available from the Wiley Online Library or from the author.

Acknowledgements

P.Y. acknowledges Prof. Wolfgang Tress for fruitful discussion while preparing this manuscript. D.P. acknowledges the financial support from the HOMING programme of the Foundation for Polish Science cofinanced by the European Union under the European Regional Development Fund

(POIR.04.04.00-00-5EE7/18-00). P.Y. acknowledges the ORSP of Pandit Deendayal Petroleum University for financial support and the financial support from DST SERB (CRG/2018/000714) and DST Nano Mission (DST/NM/NT/2018/174). A.K. and P.Y. extend their appreciation to the Deanship of Scientific Research at King Khalid University for funding this work through research groups program under grant number RGP2/86/42.

Conflict of Interest

The authors declare no conflict of interest.

Data Availability Statement

Research data are not shared.

Keywords

impedance spectroscopy, low-frequency electrochemical impedance spectroscopy, perovskites, recombination, solar cells

Received: March 24, 2021

Revised: May 10, 2021

Published online: May 28, 2021

- [1] L. Yang, C. Dall'Agnese, Y. Dall'Agnese, G. Chen, Y. Gao, Y. Sanehira, A. K. Jena, X. Wang, Y. Gogotsi, T. Miyasaka, *Adv. Funct. Mater.* **2019**, *29*, 1905694.
- [2] J. Y. Kim, J.-W. Lee, H. S. Jung, H. Shin, N.-G. Park, *Chem. Rev.* **2020**, *120*, 7867.
- [3] Best Research-Cell Efficiency Chart | Photovoltaic Research | NREL, <https://www.nrel.gov/pv/cell-efficiency.html> (accessed: March 2020).
- [4] W.-J. Yin, T. Shi, Y. Yan, *Adv. Mater.* **2014**, *26*, 4653.
- [5] Q. Dong, Y. Fang, Y. Shao, P. Mulligan, J. Qiu, L. Cao, J. Huang, *Science (80-.)* **2015**, *347*, 967.
- [6] G. Xing, N. Mathews, S. Sun, S. S. Lim, Y. M. Lam, M. Grätzel, S. Mhaisalkar, T. C. Sum, *Science* **2013**, *342*, 344.
- [7] C. Wehrenfennig, G. E. Eperon, M. B. Johnston, H. J. Snaith, L. M. Herz, *Adv. Mater.* **2014**, *26*, 1584.
- [8] W. E. I. Sha, X. Ren, L. Chen, W. C. H. Choy, *Appl. Phys. Lett.* **2015**, *106*, 221104.
- [9] C. M. Wolff, P. Caprioglio, M. Stollerfoht, D. Neher, *Adv. Mater.* **2019**, *31*, 1902762.
- [10] W. Tress, N. Marinova, O. Inganäs, M. K. Nazeeruddin, S. M. Zakeeruddin, M. Grätzel, *Adv. Energy Mater.* **2015**, *5*, 1400812.
- [11] Y. Yamada, T. Nakamura, M. Endo, A. Wakamiya, Y. Kanemitsu, *J. Am. Chem. Soc.* **2014**, *136*, 11610.
- [12] I. Zarazua, G. Han, P. P. Boix, S. Mhaisalkar, F. Fabregat-Santiago, I. Mora-Seró, J. Bisquert, G. Garcia-Belmonte, *J. Phys. Chem. Lett.* **2016**, *7*, 5105.
- [13] L. Contreras-Bernal, M. Salado, A. Todinova, L. Calio, S. Ahmad, J. Idigoras, J. A. Anta, *J. Phys. Chem. C* **2017**, *121*, 9705.
- [14] W. Tress, M. Yavari, K. Domanski, P. Yadav, B. Niesen, J. P. Correa Baena, A. Hagfeldt, M. Grätzel, *Energy Environ. Sci.* **2018**, *11*, 151.
- [15] A. R. Pascoe, N. W. Duffy, A. D. Scully, F. Huang, Y.-B. Cheng, *J. Phys. Chem. C* **2015**, *119*, 4444.
- [16] D. Prochowicz, P. Yadav, M. Saliba, M. Sasaki, S. M. Zakeeruddin, J. Lewiński, M. Grätzel, *ACS Appl. Mater. Interfaces* **2017**, *9*, 28418.
- [17] P. Yadav, M. I. Dar, N. Arora, E. A. Alharbi, F. Giordano, S. M. Zakeeruddin, M. Grätzel, *Adv. Mater.* **2017**, *29*, 1701077.
- [18] N. D. Pham, V. T. Tiong, D. Yao, W. Martens, A. Guerrero, J. Bisquert, H. Wang, *Nano Energy* **2017**, *41*, 476.
- [19] A. Riquelme, L. J. Bennett, N. E. Courtier, M. J. Wolf, L. Contreras-Bernal, A. Walker, G. Richardson, J. A. Anta, arXiv **2020**.
- [20] I. Zarazua, J. Bisquert, G. Garcia-Belmonte, *J. Phys. Chem. Lett.* **2016**, *7*, 525.
- [21] D. Moia, I. Gelmetti, P. Calado, W. Fisher, M. Stringer, O. Game, Y. Hu, P. Docampo, D. Lidzey, E. Palomares, J. Nelson, P. R. F. Barnes, *Energy Environ. Sci.* **2019**, *12*, 1296.
- [22] I. Zarazúa, S. Sidhik, T. López-Luke, D. Esparza, E. De la Rosa, J. Reyes-Gomez, I. Mora-Seró, G. Garcia-Belmonte, *J. Phys. Chem. Lett.* **2017**, *8*, 6073.
- [23] O. Almora, K. T. Cho, S. Aghazada, I. Zimmermann, G. J. Matt, C. J. Brabec, M. K. Nazeeruddin, G. Garcia-Belmonte, *Nano Energy* **2018**, *48*, 63.
- [24] P. Yadav, S.-H. Turren-Cruz, D. Prochowicz, M. M. Tavakoli, K. Pandey, S. M. Zakeeruddin, M. Grätzel, A. Hagfeldt, M. Saliba, *J. Phys. Chem. C* **2018**, *122*, 15149.
- [25] M. Saliba, T. Matsui, J.-Y. Seo, K. Domanski, J.-P. Correa-Baena, M. K. Nazeeruddin, S. M. Zakeeruddin, W. Tress, A. Abate, A. Hagfeldt, M. Grätzel, *Energy Environ. Sci.* **2016**, *9*, 1989.
- [26] C. Chen, Y. Jiang, J. Guo, X. Wu, W. Zhang, S. Wu, X. Gao, X. Hu, Q. Wang, G. Zhou, Y. Chen, J. Liu, K. Kempa, J. Gao, *Adv. Funct. Mater.* **2019**, *29*, 1900557.
- [27] F. Ebadi, N. Taghavinia, R. Mohammadpour, A. Hagfeldt, W. Tress, *Nat. Commun.* **2019**, *10*, 1574.
- [28] E. Ghahremanirad, A. Bou, S. Olyaei, J. Bisquert, *J. Phys. Chem. Lett.* **2017**, *8*, 1402.
- [29] J. Idigoras, L. Contreras-Bernal, J. M. Cave, N. E. Courtier, Ángel. Barranco, A. Borrás, J. R. Sánchez-Valencia, J. A. Anta, A. B. Walker, *Adv. Mater. Interfaces* **2018**, *5*, 1801076.
- [30] A. Pockett, G. E. Eperon, N. Sakai, H. J. Snaith, L. M. Peter, P. J. Cameron, *Phys. Chem. Chem. Phys.* **2017**, *19*, 5959.
- [31] N. E. Courtier, J. M. Cave, J. M. Foster, A. B. Walker, G. Richardson, *Energy Environ. Sci.* **2019**, *12*, 396.
- [32] S. E. J. O'Kane, G. Richardson, A. Pockett, R. G. Niemann, J. M. Cave, N. Sakai, G. E. Eperon, H. J. Snaith, J. M. Foster, P. J. Cameron, A. B. Walker, *J. Mater. Chem. C* **2017**, *5*, 452.
- [33] G. Richardson, S. E. J. O'Kane, R. G. Niemann, T. A. Peltola, J. M. Foster, P. J. Cameron, A. B. Walker, *Energy Environ. Sci.* **2016**, *9*, 1476.
- [34] D. Prochowicz, M. M. Tavakoli, M. Wolska-Pietkiewicz, M. Jędrzejewska, S. Trivedi, M. Kumar, S. M. Zakeeruddin, J. Lewiński, M. Grätzel, P. Yadav, *Sol. Energy* **2020**, *197*, 50.
- [35] M. M. Tavakoli, P. Yadav, R. Tavakoli, J. Kong, *Adv. Energy Mater.* **2018**, *8*, 1800794.
- [36] A. O. Alvarez, R. Arcas, C. A. Aranda, L. Bethencourt, E. Mas-Marzá, M. Saliba, F. Fabregat-Santiago, *J. Phys. Chem. Lett.* **2020**, *11*, 8417.
- [37] Y. Cheng, Q.-D. Yang, J. Xiao, Q. Xue, H.-W. Li, Z. Guan, H.-L. Yip, S.-W. Tsang, *ACS Appl. Mater. Interfaces* **2015**, *7*, 19986.
- [38] K. Schutt, P. K. Nayak, A. J. Ramadan, B. Wenger, Y. Lin, H. J. Snaith, *Adv. Funct. Mater.* **2019**, *29*, 1900466.
- [39] M. F. Mohamad Noh, C. H. Teh, R. Daik, E. L. Lim, C. C. Yap, M. A. Ibrahim, N. Ahmad Ludin, A. R. B. Mohd Yusoff, J. Jang, M. A. Mat Teridi, *J. Mater. Chem. C* **2018**, *6*, 682.
- [40] K. Mahmood, S. Sarwar, M. T. Mehran, *RSC Adv.* **2017**, *7*, 17044.
- [41] D. Prochowicz, M. M. Tavakoli, A. Solanki, T. W. Goh, K. Pandey, T. C. Sum, M. Saliba, P. Yadav, *J. Mater. Chem. A* **2018**, *6*, 14307.

- [42] D. Prochowicz, R. Runjhun, M. M. Tavakoli, P. Yadav, M. Saski, A. Q. Alanazi, D. J. Kubicki, Z. Kaszukur, S. M. Zakeeruddin, J. Lewiński, M. Grätzel, *Chem. Mater.* **2019**, *31*, 1620.
- [43] T. S. Sherkar, C. Momblona, L. Gil-Escrig, J. Ávila, M. Sessolo, H. J. Bolink, L. J. A. Koster, *ACS Energy Lett.* **2017**, *2*, 1214.
- [44] A. Castro-Méndez, J. Hidalgo, J. Correa-Baena, *Adv. Energy Mater.* **2019**, *9*, 1901489.
- [45] D. J. Kubicki, D. Prochowicz, A. Hofstetter, M. Saski, P. Yadav, D. Bi, N. Pellet, J. Lewiński, S. M. Zakeeruddin, M. Grätzel, L. Emsley, *J. Am. Chem. Soc.* **2018**, *140*, 3345.
- [46] S. Wu, Z. Li, J. Zhang, T. Liu, Z. Zhu, A. K. Jen, *Chem. Commun.* **2019**, 55, 4315.
- [47] J. Yao, H. Wang, P. Wang, R. S. Gurney, A. Intaniwet, P. Ruankham, S. Choopun, D. Liu, T. Wang, *Mater. Chem. Front.* **2019**, *3*, 1357.